Pre-print of article that appeared at WACV 2008.

The published article can be accessed from:
http://ieeexplore.ieee.org/xpl/freeabs_all.jsp?arnumber=4543999

INSPEC^{2}T: INEXPENSIVE SPECTROMETER COLOR CAMERA TECHNOLOGY

W. J. Scheirer[1,2]*, S. R. Kirkbride*[1]*, and T. E. Boult*[1,2]

[1]VAST Lab, University of Colorado at Colorado Springs and [2]Securics, Inc.
Colorado Springs, CO.

ABSTRACT

Modern spectrometer equipment tends to be expensive, thus increasing the cost of emerging systems that take advantage of spectral properties as part of their operation. This paper introduces a novel technique that exploits the spectral response characteristics of a traditional sensor (i.e. CMOS or CCD) to utilize it as a low-cost spectrometer. Using the raw Bayer pattern data from a sensor, we estimate the brightness and wavelength of the measured light at a particular point. We use this information to support wide dynamic range, high noise tolerance, and, if sampling takes place on a slope, sub-pixel resolution. Experimental results are provided for both simulation and real data. Further, we investigate the potential of this low-cost technology for spoof detection in biometric systems. Lastly, an actual hardware systhsis is conducted to show the ease with which this algorthim can be implemented onto an FPGA.

1. INTRODUCTION

Obtaining sufficient spectral resolution and sufficient dynamic range in spectrometers has, until now, required a higher resolution linear CCD with 10-bit or 12-bit resolution. Little economy of scale can be achieved, because these are such low volume components. Thus, the cheapest available units cost over $3,000, with most applications using a device priced around $7,000. The need for lower cost spectrometer equipment is apparent in several, very different domains.

The biometrics community is most interested in low-cost spectral analysis, and has been instrumental in developing spectral intensity matching techniques. Useful attacks against biometrics have been widely reported in [1] [2] [3], forcing security engineers to take appropriate precautions against false body parts and behaviors. In particular, fingerprint recognition is a popular method for authentication and recognition, but is also very susceptible to attack. Spectral imaging for spoof detection is not new [4] [5], but a low-cost solution for an enrollment/verification system has yet to emerge.

Determining the exact wavelength positions in the imagery is another problem of interest. Calibration and characterization of CCDs used for spectral imagery is of interest to researchers [6] [7] and [8]. Because the positions will vary based on the CCD used, calibration based on known light sources is often used. Since the intent here is to use color imagery (traditionally, intensity has been used for spectral imagery), it may be possible to map color to wavelength more easily.

Beyond biometrics and sensor considerations, lower cost spectrometers can be deployed in many areas where higher cost equipment is currently in service. Industrial manufacturing and printing, specifically, quality control for color (dyes, inks, and various other pigments) evaluates spectral data. If one can drive down the cost of the production process, or make a scalable process feasible, companies can produce a cheaper product, while maintaining the quality. Many industrial/commercial products, especially copiers and scanners, already contain low-cost sensor parts for traditional imaging purposes. Enhancing existing designs to take advantage of imaging systems that can provide the spectral data we're looking for is very possible. Recent work [9] [10] [11] considers spectral reflectance measurement and associated device calibration, with the very recent work of [9] utilizing RGB sensors to do so. In another example of industrial quality control, screening for the presence of unintended harmful materials, such as the case of lead in toys, can also be accomplished.

Another proposed application area is in microscopy. If target cells are dyed, and let to circulate through a biological system, their later identification is desirable. Using the technique proposed in this paper, it would be possible to forgo construction of a complete multispectral image for an individual cell, or group of cells, and instead rely on a spectrograph taken from a point on a cell. The time saved when analyzing thousands of cells would be significant.

We also envision this technology would be valuable for general laboratory science in the UV to near-IR bands, especially for educational institutions, where equipment budgets are constrained.

In another, potentially lifesaving application, a low-cost spectrometer can be used as a replacement for breathalyzer technology. In a variation on known spectral measuring systems [12] [13] utilizing LED illumination technology similar to [14] [15] to prevent drunk driving, we propose correlating blood oxygenation with light absorption, so an intoxication measurement can be made by mapping spectral response to a blood-alcohol level. This technology can be completely

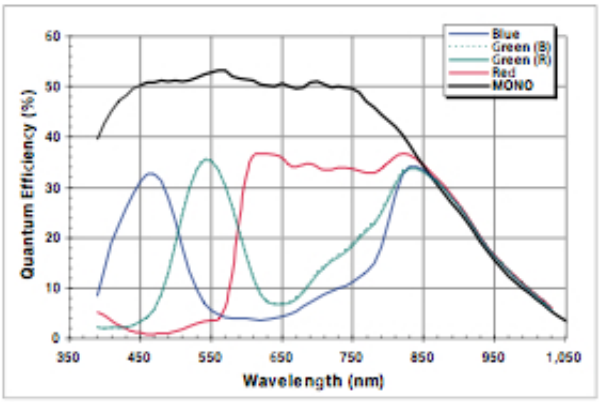

Fig. 1. Spectral Response Characteristics for the Micron MT9V022 CMOS sensor

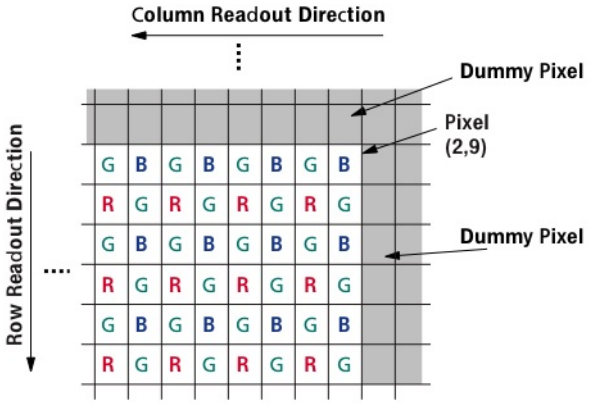

Fig. 2. Typical Bayer Pattern

non-invasive, and, if coupled with a biometric entry system, does not carry the same stigma as current interlock technology for vehicles. Without a per cost use commonly found in this area, a low-cost spectrometer system can be deployed for under $100.

The rest of this paper is as follows. In Section 2 we describe the design of our low-cost spectrometer. Three different advantages of the design are discussed, including wide dynamic range, noise tolerance, and subpixel resolution. In Section 3, simulation results are presented for a set of artificial spectral data to compare to straight intensity imaging, and to show the subpixel resolution technique. Bringing the experiments out of simulation, we test a set of real light sources in Section 4, and conduct a biometric spoof detection experiment in Section 5. Finally, in Section 6, we describe an actual hardware implementation of the techniques presented.

2. DESIGNING A LOW-COST SPECTROMETER

At the very core of our approach is the Bayer color pattern [16], coupled with the spectral response characteristics of the commodity sensor at hand. As depicted in Figure 1, the spectral response curve for a sensor provides a mapping between wavelengths and associated quantum efficiency. For single chip color sensors (i.e. CCD or CMOS), individual pixels have colored filters. For these sensor, depending on the wavelength incident on a red, green, or blue pixel, the pixel will register an intensity value proportional to the corresponding quantum efficiency. Single chip cameras commonly use the Bayer pattern (Figure 2), containing 50% green, 25% red, 25% blue, coupled with a demosaicing scheme for color imagery. In our approach, the different spectral responses of the raw Bayer data are exploited to both estimate the brightness of the sample, as well as to determine the wavelength of measured light at that point. Unlike regular imaging applications, the dispersive filter will separate light, and, with calibration, we can know what range of wavelengths are expected at any particular location. We exploit this in three different ways.

First, as is evident in the response curves of Figure 1, at any particular wavelength, the response of different pixels is significantly different. For example, if at 650nm, the incident illumination is sufficient to cause the red channel to saturate, we will still be able to measure the green and the blue, which have much lower response at that wavelength, by a factor of 4 and 8 respectively, hence adding 4 additional bits to the effective dynamic range. For, CCD and CMOS sensors, this technique can add significantly to the measurable dynamic range, *within* the visible spectrum. A similar approach for digital micromirror arrays was used in [17], and with spatially varying pixel exposures in [18]. We can utilize the technique [18] because we know the expected wavelength from calibration. In comparison to existing technology, this level of dynamic range is achieved by high-end systems integrating cooled linear arrays, costing thousands of dollars.

Second, if we design the physical spectrometer device to produce a strip on the sensor (with a traditional slit spectrometer, or by spreading a spot into a line with a cylindrical lens), we will have multiple measurements for each pixel type for each spectral line. We can combine data (i.e. take the mean) to reduce random sensor noise, as well as trim the tails of each line to reduce extreme variation from the mean (spatial non-uniform distortion). It is important to note that we are exploiting the fact that from the calibration of the color separation/dispersion pattern we know what range of colors should be incident on a pixel, and hence know which measurements can be combined.

Third, we can realize another advantage if, rather than aligning spectral lines directly along the rows or columns, we intentionally image them at an angle along the 2D array (Figure 3. By combining the 2D nature of the sampling grid with a

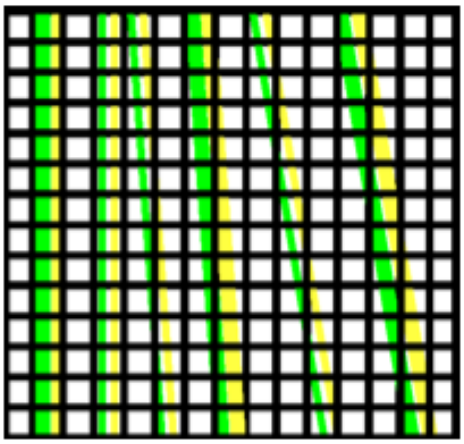

Fig. 3. If cells averaged their content, the left most pairs would produce constant data. Sampling of the sloped lines provides sufficient information to determine there are 2 lines, and even to estimate the width of those lines.

slanted linear pattern we can provide for subpixel reconstruction, effectively improving the sampling resolution by a factor of 8 or more. Combining the slope-based computations with the spatial varying exposure uses data in multiple ways and to balance noise with increased resolution the preferred embodiment only gains a factor of 8 in resolution. This technique becomes more interesting with the observation that, typically, when we sample, we will not have perfect alignment between intensity for a particular wavelength and a column of pixels where we expect the wavelength. Thus, we can gain an advantage from a seeming disadvantage in alignment.

In applications such as spoof detection for biometric systems and industrial manufacturing, recovery of the spectrum is followed by matching with a pre-stored spectral signature. If the application's only purpose for the spectrum is matching, then we have a new alternative, *direct multi-colored spectral signature matching*. Rather than finding a super-resolution spectrum or fitting the parameters of a discrete model, we use the raw Bayer data to represent the signature. Because the raw data is sufficient to reconstruct the super-resolution spectrum, if an appropriate matching metric can be applied, it could provide for equivalent matching quality without the computational costs of doing super-resolution or non-linear optimizations.

Further considerations are made with respect to the design of the physical device. To split light into its respective spectral components, a grating or prism must be used. At the cheapest end, holographic diffraction gratings in the range of 500 lines/mm and 1000 lines/mm are very common, and extremely inexpensive (less than $5 per 6" x 12" sheet). More expensive Echelle gratings (around $100 for a single, small sheet) provide for multiple diffraction orders via a system of two gratings, producing spectrograms that are usually slanted - useful for the subpixel reconstruction problem described above. Beyond gratings, a newer technology, spherical beam volume holograms, can be used to perform the job of a slit, first lens, grating, and second lens in a spectrometer. With this, a sensor is simply attached, leading to a full spectral imaging package. This technology is still experimental, but is a likely candidate for low-cost spectral systems as it matures.

As mentioned in Section 1, the likely deployment of this design will be in existing commercial and industrial devices where spectrometer equipment has traditionally been too expensive to use. Thus, image processing will likely take place in an embedded platform. Bayer conversion in hardware is not a new innovation, with image enhancement available for both CMOS [19] and CCD [20] sensors. Typically, the raw Bayer data is demosaiced, before gamma correction, color correction, white balancing, and contrast enhancement is applied. By dedicating part of the hardware to perform the spectral analysis before the demosaicing, existing designs can be converted to dual-use (think of a biometric imaging system that can both sample a finger, and perform spectral spoof detection). The cost of an FPGA based image processing system would be between $10 - $15.

3. SIMULATION RESULTS

In simulation, we were primarily concerned with answering two questions: 1. How well does the Bayer technique compare with 2D intensity imaging? 2. Can we achieve subpixel resolution by imaging on a slope?

For many applications, spectral signature matching is a useful operation. The premise is to take a high quality sample of a known material, and use its spectral response as a comparison for unknown materials, or material verification. Most systems simply use a grayscale image, and compare intensity values of a sample to the signature image. The noise tolerance of linear intensity arrays is easy to consider. With only one row of pixels, there is no additional data to consider for a particular wavelength. Thus, a sample tainted by noise can only be corrected if a pre-defined noise model is known during image processing. 2D sensors provide more detail. Using the Bayer pattern, we have even more detail with each three color pixel block, and can match signatures at roughly the same rate, or better, compared to more robust 2D intensity image matching. The signature matching simulations utilize the spectral characteristics of a Micron MT9V022 CMOS sensor.

Spectral signature matching was tested between Bayer pattern and grayscale simulation images representing discrete spectral bands. In each case, the Bayer pattern method performed as good, or better than the performance of the grayscale matching method. For each grayscale image, and its corresponding Bayer pattern image, 30 standard normal additive noise levels were applied, from $\sigma = 1$ to $\sigma = 30$, for a total of 300 images.

Image	Gaussian noise (σ)
Bayer 1	17
Intensity 1	16
Bayer 2	20
Intensity 2	16
Bayer 3	28
Intensity 3	23
Bayer 4	17
Intensity 4	16
Bayer 5 (spatial non-uniform distortion)	8
Intensity 5 (spatial non-uniform distortion)	12

Table 1. Signature matching between Bayer and Intensity spectrum pairs. 30 standard normal additive noise levels were applied. In all cases, the Bayer technique performs comparably, if not better to intensity matching.

Each noisy image was run through a Bayer signature matching algorithm, and a grayscale matching algorithm (simple intensity matching), both incorporating noise handling via taking the mean of each wavelength column, and trimming the tails of extreme values. Each matching algorithm keeps track of mismatched pixel intensity values; in the case of the Bayer data, colors are aligned against each other for matching. If the mismatched pixel count exceeds at predefined threshold (in our testing, 5%), then we consider the test image to not match the signature image.

The results for 5 image pairs are presented in Table 1. The second column represents the noise limit where matching was still possible. The last pair, 5, with spatial nonuniform distortion plus gaussian noise, is the only instance where the Bayer imagery performs slightly weaker (though comparably) to the intensity image.

Simulating sub-pixel resolution is accomplished by considering a situation similar to the right most spectral lines of Figure 3, that is, intentionally imaging the spectral lines at a small slant. In the previous noise experiments 1 pixel width was considered the equivalent of 1nm of wavelength. This approximation can further be refined by recognizing that only a fraction of each wavelength is exciting the pixel when the spectral lines are imaged at a slant. Figure 4, represents this situation. If Figure 1 is considered continuous, then the predicted values between each 1nm wavelength can also be modeled. When taking these modeled values at the detected wavelength, found through physical calibration, the sub-wavelength values can be interpolated by considering a system of linear equations. Given the distributional model of spreading, the expected values can be extracted and then used to estimate the actual values with the sub-pixel resolution desired. It is important to notice that for the upper portion of the image pixel values for 3 and 4 fall away. This can be seen quite clearly in Figure 4. Correspondingly, on the lower half of the figure pixel measurements for 1 and 2 fall away. Not also how this can be important if the central line would have saturated the center pixel.

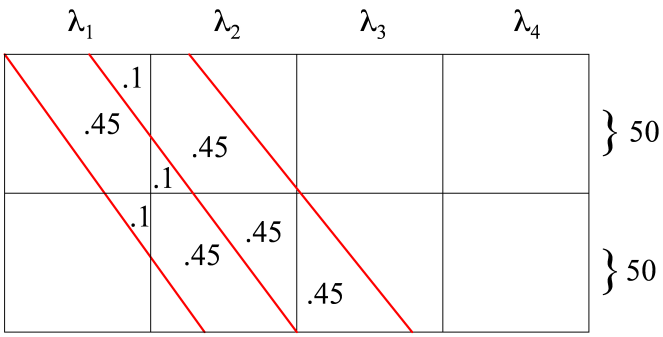

Fig. 4. Example pixel orientation of sloped spectral lines in a total region consisting of 2 rows and 50 columns ($slope = 25$). Spectral data covers 5 different pixels, in varying area size per subpixel region. By considering the theoretical value of this subpixel regions (as shown) and measured subpixel regions after sampling, we can achieve subpixel resolution.

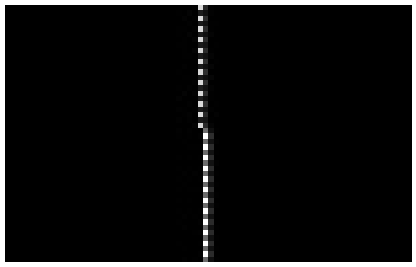

Fig. 5. Test image with slope=25

Figure 5 is a sample image with a slope of 2 (representing a realistic, unintentionally sloped sample). We presume the image has a spectral resolution of 1 pixel per 2 wavelengths. By applying the above method, with an ideal goal of 10 spectral components, we can separate 10 2-angstrom wide spectral components for each pixel column of sampled data. This gains a factor of 10 in resolution. Figure 6 shows a spectrogram with blurring between 651nm and 652nm for a red laser (expected spectral response around 650nm, according to equipment specification) imaged at, roughly, a 2 degree slant.

4. LIGHT SOURCE RESULTS

Real experimental data was gathered using a Sony ICX084 CCD sensor, configured to capture images in raw Bayer mode. In front of the sensor, a diffraction grating of 500 lines/mm

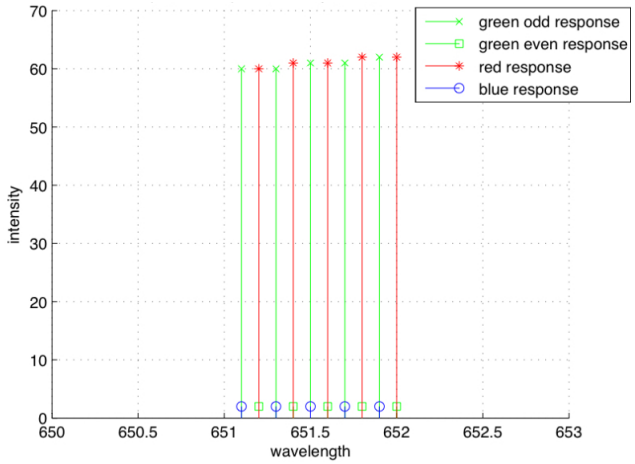

Fig. 6. Spectrogram for a red laser imaged at roughly a 2 degree slant. Note the blurring between 651nm and 652nm. If actual positions are known, super resolution can be achieved from this data.

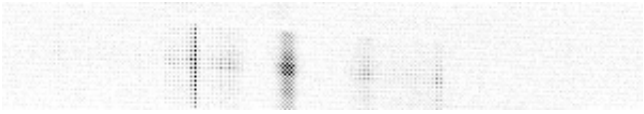

Fig. 7. The discrete spectrum of a cold compact fluorescent tube light

was used to split light into its spectral components. Ten different light sources were sampled: mercury fluorescent, laser, halogen at a low intensity, halogen at a medium intensity, halogen at a high intensity, green LED, yellow-green LED, Orange LED, Yellow LED, White LED (the LEDs emit a continuous spectrum, as opposed to some older LEDs, that emit a very discrete spectrum). These sources represent both discrete (for example, Fig. 7) and continuous spectra (for example, 8). Computed spectrograms produced results consistent with known spectral responses, as shown in Fig. 10. We note that the reference spectrum in Fig. 9 is one of many CFL spectra, with each manufacturer uses its on mix which produces different spectra. Our CFL is a hand-held flashlight and not expected to match exactly, but the prominent spectral signature, the prominent mercury lines at 436nm and 546nm, are well recovered. The limited calibration data from Sony limited our experiments to spectral responses in the range of 400nm - 700nm. Experimentation showed the sensor was capable of registering light in the UV and near-IR bands, thus hinting at the potential of sensing beyond the visual spectrum at a very low cost.

The ability to estimate intensity in saturated wavelength ranges is a core piece of our design. Thus, we demonstrate it with experimental samples of laser light, where red saturates

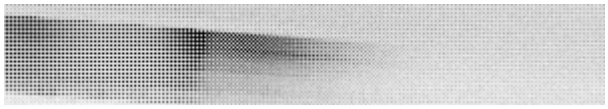

Fig. 8. The continuous spectrum of halogen light

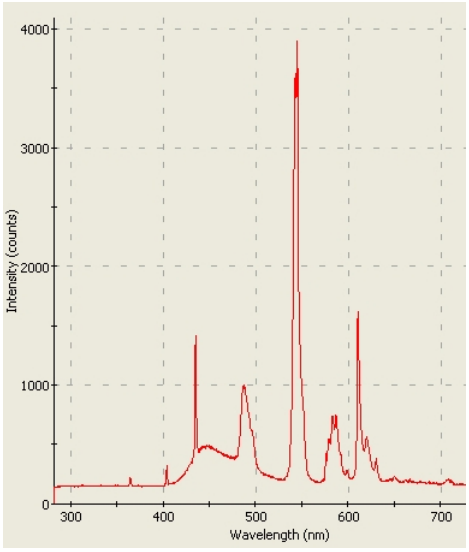

Fig. 9. Reference spectrograph of a cold compact fluorescent tube light. Image Credit (adapted): home.att.net/∼ledmuseum/spectra7.htm

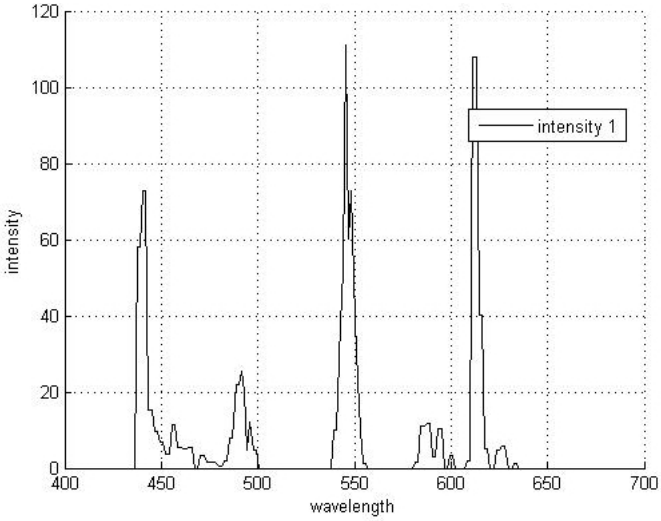

Fig. 10. Computed spectrogram for the the sampled cold compact fluorescent tube light of Fig. 7

Source	Gaussian Noise (σ)	S&P Noise (density)	Spatial Nonuniform Distortion (rows)
Mercury Fluorescent	15	3	10
Laser	15	2	10
Halogen Low	15	4	6
Halogen Medium	15	10	6
Halogen High	15	10	6
Green LED	13	2	12
Yellow-Green LED	15	3	10
Orange LED	15	10	6
Yellow LED	15	8	7
White LED	15	10	7

Table 2. Noise tolerance of 10 different light sources

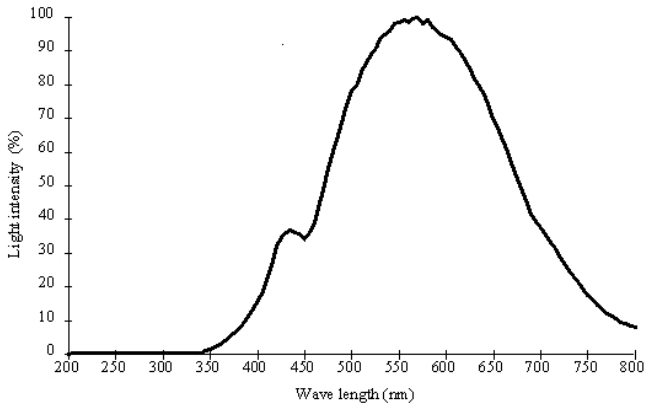

Fig. 11. Reference spectrograph for halogen light. Image Credit (adapted): www.fojo.org/papers/mepsoxygen/index_files/image026.gif

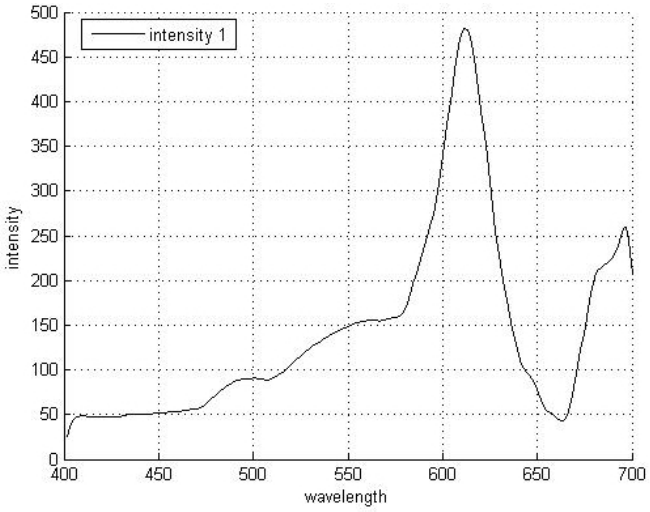

Fig. 12. Computed spectrogram for the the halogen light of Fig. 8. Note the increase in dynamic range beyond 8 bits.

around 600nm. In red's saturation range, we can still measure green (both Gb and Gr) and blue, allowing us to estimate the true value of red. By considering all three colors, we can estimate the general intensity of the spectral response across all measurable wavelengths, providing information where saturation had previously occurred. Figure 12 shows the computed spectrogram for the sampled halogen light of 8. An increase in dynamic range beyond 8 bit (maximum intensity value of 255) can clearly be seen, as the peak of the curve extends beyond 450 at around 620nm. Compared to the reference spectrum in Fig. 11, there is some variation. There are several reasons for this. First, the dip and subsequent rise of the curve between 650nm and 700nm is caused by the green intensity increasing, as the modeled response decreases, with green being used to model the red response. Second, the continuous nature of the halogen spectrum proves to be more difficult in experimentation than the discrete spectrum of fluorescent light. Error from the sensor's modeled spectral response characteristics, coupled with error introduced by the experimental apparatus account for the rest of the deviation.

Noise tolerance results, while in general lower than the simulation results, are still quite promising. We tested three different types of noise, including guassian from $\sigma = 1$ to $\sigma = 15$, S&P noise from density=1 to density=10, and spatial non-uniform noise from row=1 to row=15, for a total of 400 test images. From Table 2, we observe a very high tolerance for gaussian noise, and a strong tolerance for S&P and spatial non-uniform noise. From the data, there is an inverse relationship between S&P and spatial non-uniform noise, in terms of tolerance. Discrete spectra and tightly clustered wavelengths with lower intensity for spectral response (mercury fluorescent light, laser, green LED, yellow LED) are impacted strongly by low densities of S&P noise, because of their wavelength arrangements. Conversely, these spectra tolerate local row distortion bands much better, as they do not possess the amount of lower intensity spectral responses that more continuous spectra do, thus, they do not lose as much information with increased spectral data loss. Nearly all sources tolerate gaussian noise well, because the spectral data combination for three colors is rather robust.

5. SPOOF DETECTION FOR BIOMETRIC SYSTEMS

An important application area for a low-cost spectrometer is spoof detection for biometrics. We performed three experiments, sampling the reflectance of light off skin, skin covered with gelatin "fingerprints", and skin covered with gelatin "fingerprints" mixed with chicken blood (meant to fool current spoof detection technology by closer resembling the material of the finger). Red laser light, at 650nm, and green laser light, roughly between 545nm and 555nm, were used in this experiment.

For the experimental process, subjects placed their fingers over the light, with and without the spoofing material present. Light passing through the finger was sampled after passing through our slit spectrometer. In total, 90 fingers were sampled, from a diverse range of subjects (Caucasian, African-American, Asian) to account for variability in skin color.

Results of this experiment are shown in Figure 13. We measured intensity as a function of absorption by material. For each sample set, all samples were averaged, with real fingers absorbing the most light, and gelatin and gelatin mixed with blood samples reflecting noticeably more light, The differences are dozens of standard deviations, stastically very signfinicant compared to the variations across populations. We can conclude that this technique is effective for spoof detection in biometric systems.

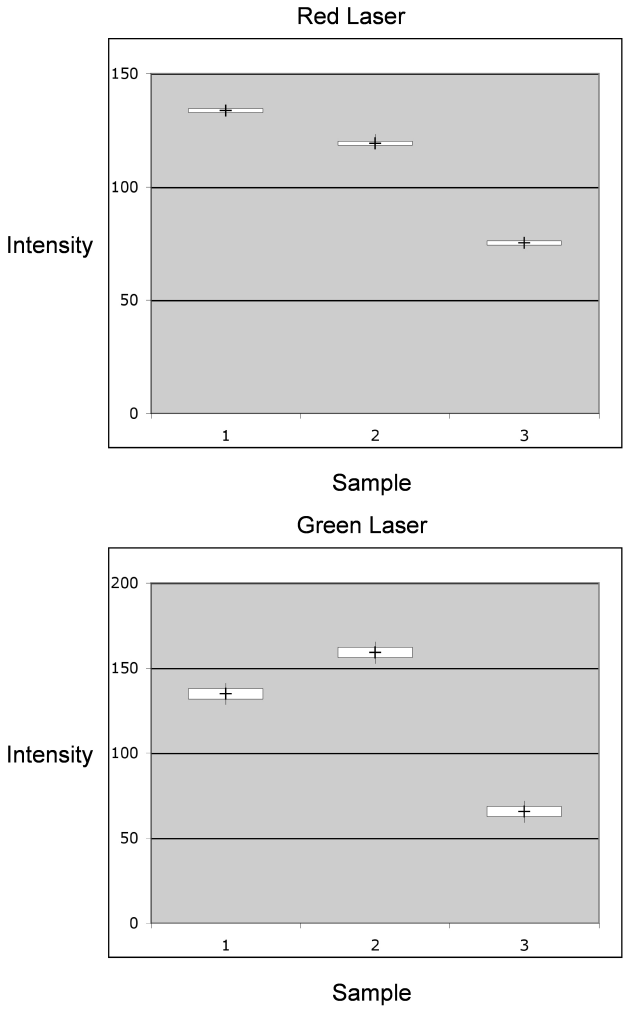

Fig. 13. From left to right: gelatin, gelatin mixed with blood, and real fingers. The mean, and two standard deviations from the mean are shown.This difference between sample types is significant enough to detect spoofing attacks against biometric systems.

6. HARDWARE IMPLEMENTATION

The algorithm to process the spectral lines is straight forward. There are several steps to the process. First, the various pixel types: Green, Red and Blue are sorted into appropriate bins. Next, an average of all the intensities of the sorted pixels is taken. Lastly, this data is output serially. To implement this process on an FPGA several basic devices are constructed.

There are two main parts to the implementation: the Finite State Machine and the front end logic. First, a state machine in the form of a ring counter is used to sort the pixels into various bins. As the state machine is sorting the data is being added together in an accumulator. While this is occurring a counter counts the clock cycles, which corresponds to the number of pixels sorted. Then, another module divides the number of summed intensities by the number of pixels counted to get an average value. This value is output via the serial port. The FSM consists of four D flip-flops. It was designed using the one-hot encoding method. The negation of the output of the last D flip-flop is tied into the input of the first D flip-flop.

The output of this state machine is tied into the front end logic module. The first level of the front end logic module "ands" the input data with the output of the state machine. When the machine is in the appropriate state the data gets sorted into the correct accumulator, of which there are four. Each accumulator represents a pixel type and is accompanied by a counter. The accumulator is simply a register fed back into a summing function, driven by the clock. The output of the accumulator is divided by the number output by the counter. The output can then be used by the techniques mentioned above to gain increased resolution and better accuracy than other much more expensive spectrometers.

7. CONCLUSION

In this paper, we have introduced a novel technique for using common sensors as low-cost spectrometers. The low-cost spectrometer design supports wide dynamic range, high noise tolerance, and sub-pixel resolution. Promising results were

presented from experiments using simulation and real data, highlighting the three key advantages, and the technique's improvement over traditional intensity imaging. Further, we presented experimental data for a biometric spoof detection application, with very promising results for detecting false fingerprints, including those meant to mimic real fingers closely. In terms of the actual implementation presented and cost, the system can be implemented directly into an FPGA, at $10-$15, with a CCD or CMOS for imaging, at $10-$20, delivering an attractive low-cost solution for a variety of applications.

8. REFERENCES

[1] M. Faundez-Zanuy, "On the vulnerability of biometric security systems.," *IEEE Aerospace and Electronic Systems Magazine*, vol. 19, no. 6, pp. 3–8, 2004.

[2] T. van der Putte and J. Keuning, "Biometrical fingerprint recognition don't get your fingers burned," in *Proceeding of the Fourth Working Conference on Smart Card Research and Advanced Applications*, 2000, pp. 289–303.

[3] T. Matsumoto, H. Matsumoto, K. Yamada, and S. Hoshino, "Impact of artificial gummy fingers on fingerprint systems," in *Proceedings of SPIE Optical Security and Counterfeit Deterrence Techniques IV*, 2002, p. 4677.

[4] M. Ennis, R. Rowe, S. Corcoran, and K. Nixon, "Multispectral sensing for high-performance fingerprint biometric imaging," in *Lumidigm White Paper*, 2005.

[5] K. Nixon and R. Rowe, "Multispectral fingerprint imaging for spoof detection," in *Proceedings of SPIE Conference on Biometric Technology for Human Identification, Orlando, USA*, 2005, vol. 5779, pp. 214–215.

[6] G. Polder, G. van der Heijden, P. Keizer, and I. Young, "Calibration and characterization of imaging spectrographs," in *Proceedings of the 2001 Multi-spectral and hyperspectral image acquisition and processing, Wuhan, China*, 2001, pp. 310–319.

[7] J. Mullikin, L. van Vliet, H. Netten, F. R. Boddeke, I. T. van der Feltz, and G. Young, "Methods for ccd camera characterization," in *Proceedings of the 1994 SPIE Conference on Image Acquisition and Scientific Imaging Systems*, 2003, pp. 73–84.

[8] H. M. G. Stokman, Th. Gevers, and J. J. Koenderink, "Color measurement by imaging spectrometry," *Computer Vision and Image Understanding: CVIU*, vol. 79, no. 2, pp. 236–239, 2007.

[9] J. Park, M. Lee, M. Grossberg, and S. Nayar, "Multispectral imaging using multiplexed illumination," in *In Proc. of the 11th IEEE International Conference on Computer Vision, Rio De Janeiro, Brazil*, 2007.

[10] K. Barnard and B. Funt, "Camera characterization for color research," *Color Research and Applications*, vol. 27, no. 3, pp. 152–163, 2002.

[11] M. Vrhel and H. Trussell, "Color device calibration: A mathematical formulation," *IEEE Transactions on Image Processing*, vol. 8, no. 12, pp. 1796–1806, 1999.

[12] D. Edmonds and J. Hopta, "Driver alcohol ignition interlock, U.S. Patent No. 6 229 908," 2001.

[13] L. Duval, "Substance detection and alarm using a spectrometer built into a steering wheel assembly, U.S. Patent No. 7 173 536," 2007.

[14] I. Fryc, S. W. Brown, and Y. Ohno, "Spectral matching with an led-based spectrally tunable light source," in *In Proc. SPIE Fifth International Conference on Solid State Lighting*, 2005, vol. 5941, pp. 289–297.

[15] M. Vrhel, "An led based spectrophotometric instrument," in *In Proc. SPIE, Color Imaging: Device-Independent Color, Color Hardcopy, and Graphic Arts IV*, 1998, vol. 3648, pp. 226–236.

[16] B.E. Bayer, "Color Imaging Array, U.S. Patent No. 3 971 065," 1976.

[17] S. Nayar, V. Branzoi, and T. Boult, "Programmable imaging using a digital micromirror array," in *Proc. of IEEE Conf. on Comp. Vision and Pattern Recognition*, 2004, vol. 1, pp. 436–443.

[18] S. Nayar and T. Mitsunaga, "High dynamic range imaging: Spatially varying pixel exposures," in *Proc. of IEEE Conf. on Comp. Vision and Pattern Recognition*, 2000, vol. 1, pp. 472–479.

[19] M.F. Tappen, B.C. Russell, and W.T. Freeman, "Exploiting the sparse derivative prior for super-resolution and image demosaicing," in *Proc. Third Intl Workshop on Statistical and Computational Theories of Vision*, 2003.

[20] H. Zen, T. Koizumi, H. Yamamoto, and I. Kimura, "A new digital signal processor for progressive scan ccd," *IEEE Trans. Consumer Electronics*, vol. 44, no. 2, pp. 289–296, 1998.